ELSEVIER

Contents lists available at ScienceDirect

Acta Materialia

journal homepage: www.elsevier.com/locate/actamat



Full length article

A new approach to solid-state nucleation in kinetically-constrained systems

Christopher Hutchinson*, Yves Brechet

Department of Materials Science and Engineering, Monash University, Victoria, 3800, Australia

ARTICLE INFO

Keywords: Clusters Nucleation Precipitation Phase transformations

ABSTRACT

Nucleation is the first step of the phase transformations that we use to control the microstructures of engineering materials. The starting point for questions of nucleation is usually Classical Nucleation Theory (CNT) but for solid-state nucleation at low temperatures where atomic mobility is limited, such as in engineering alloys, CNT has not been very successful is quantitatively predicting nucleation. A strong assumption of CNT is that all thermally-induced stochastic fluctuations, no matter how far their compositions lie from the bulk alloy composition, are possible and that they become nuclei when a critical size determined from thermodynamics is reached.

Here we present a new and complementary model for solid-state nucleation. We consider the other extreme where atomic mobility is limited and thermally-induced stochastic clusters cannot form in the time scale relevant for a nucleation event. Instead, we consider the geometric clusters that are a statistical feature of any solution as the origin of the nuclei and present a simple model for the number of nuclei and their rate of 'activation'. This new 'geometric cluster' model is shown to be able to successfully predict the competition in phase nucleation during the crystallization of a series of Al-Ni-Y metallic glass, predict the solvent trapping that is increasingly seen in solid-state nucleation and predict the peak number density of precipitates observed in Cu-Co and Fe-Cu alloys.

1. Introduction

Nucleation is the first stage of one phase forming from another. It occurs all around us in nature (e.g. droplets of rain forming in cloud vapor) but it is also represents the first step of the phase transformations that occur in man-made materials such as engineering alloys. Since phase transformations are one of the most powerful ways to manipulate the micro and nanostructure of engineering materials, and therefore influence their properties, controlling nucleation is critical to materials and microstructure design. The kinetics of nucleation often sets the lower bound on the characteristic length scale of the microstructure and this affects many important materials properties. The rate of nucleation of solid grains in a liquid during solidification determines the lower bound of the grain size in the as-cast state. The rate of nucleation of precipitates in an alloy during solid-state precipitation determines the minimum precipitate spacing. In both cases, these length scales strongly influence the mechanical properties (e.g. strength). In the case of nanostructured magnetic materials formed by the crystallization of a metallic glass, nucleation must be controlled so that the correct phase, with the correct size and volume fraction appears for the material to exhibit the desired magnetic properties (e.g. coercivity).

Ideally, a model for nucleation should be able to predict, from the thermodynamically permissible phases, which phase will nucleate first during a phase transformation (including the composition of the phase), and the kinetics of nucleation.

The starting point for questions of nucleation in materials science is usually Classical Nucleation Theory (CNT), e.g. [1–3]. CNT describes nucleation as the transient formation of clusters with the crystal structure (and chemistry) of the new phase by thermally-induced stochastic fluctuations until a cluster attains a size exceeding the 'critical' size, R*, (associated with a critical energy barrier, ΔG^*). It is an energetically up-hill process until R* is exceeded, after which the nucleus may enter the growth stage. The stochastic formation of clusters requires atomic mobility and the degree of mobility is very different in different systems. In gases and liquids, the mobility may be high, but in solid-state nucleation, especially at low temperatures, atomic mobility can be uniformly very limited and also vary significantly from one chemical species to another. It is exactly these conditions of solid-state nucleation which are emphasised in this contribution.

The appeal of CNT is its simplicity and that it correctly captures the

E-mail address: crh@monash.edu (C. Hutchinson).

^{*} Corresponding author.

intuitive qualitative trends expected for a given nucleating phase [1–3]. At a given temperature, as the thermodynamic driving force for nucleation increases (leading to a decrease in the energy barrier ΔG^*), the nucleation rate of a given phase increases. As the interfacial energy decreases, the nucleation rate increases. For a given alloy composition, as the temperature changes, a competition between atomic mobility and the thermodynamic driving force for nucleation occurs which can lead to a non-monotonic dependence of the nucleation rate on temperature.

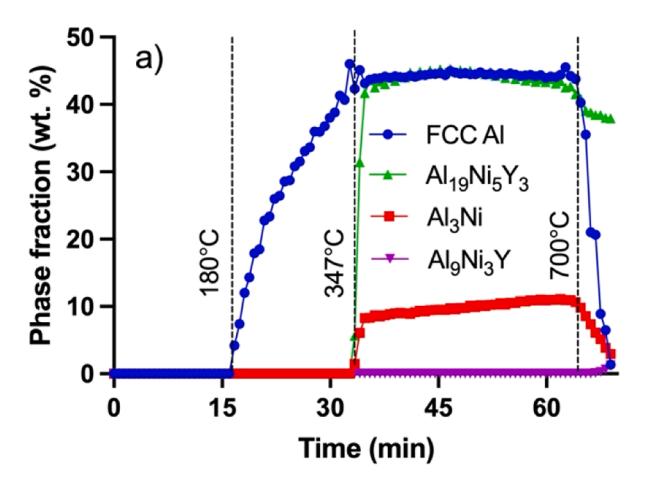
However, when one tries to quantitatively compare CNT with experimental data from solid-state phase transformations, problems appear. CNT is extremely sensitive to the interfacial energy of the phase nucleating, but even when the interfacial energy is 'tuned' by fitting CNT to experimental data for a given set of conditions (e.g. alloy composition and temperature), the ability to quantitatively predict the solid state nucleation rate in conditions slightly different to those used for calibration (e.g. slight change in temperature or alloy composition), is poor. This is true even in the alloy systems where CNT is thought to have the best chance of success, e.g. precipitation of low misfit, spherical Co particles in a Cu matrix, e.g. [4]. With the increasingly widespread availability of thermodynamic and kinetic databases, and the availability of better and better experimental data (e.g. from combinatorial experiments), more researchers are building kinetic models for solid-state phase transformations (e.g. precipitation processes), and the inability to quantitatively describe the experimental kinetics of nucleation is exposing important limitations of CNT.

The difficulties in quantitatively describing solid-state nucleation using CNT have long been known by those studying the crystallization of metallic glasses, e.g. [5,6]. In the case of well-defined crystals forming in an amorphous metallic matrix, reasonable estimates of the interfacial energies can be made and researchers quickly realised that CNT could not explain the high number densities of crystals that formed during devitrification of metallic glasses. Instead, researchers would invoke the idea of "pre-existing structural and/or chemical heterogeneities" as a means of explaining the high number densities of phase formed, e.g. [5–7]. Such heterogeneities have been experimentally shown to exist, e. g. [7,8], and are also observed in numerical simulations, e.g. [9].

Some might argue that given the extreme sensitively of CNT to the interfacial energy of the nucleating phase, and the assumptions and simplifications made in deriving the CNT rate equation, it is unfair to expect quantitative agreement with experiments in real systems, especially in the solid-state. However, even if we look only at qualitative predictions of which phase nucleates first, amongst an array of competing phases, we find that CNT is unable to correctly predict the competition in phase formation. Consider the example shown in Fig. 1a of the crystalline phases that form in an Al-9Ni-4Y metallic glass when

heated [10]. These experiments were performed using in-situ heating in a synchrotron beam so the order of phase formation could be monitored quantitatively. Experimentally, the first crystalline phase to form in this metallic glass is FCC Al at a temperature of $\sim \! 180$ °C. From the lattice parameter of the FCC it is known to be almost pure Al [10]. Al-Ni-Y is a system where a good thermodynamic description exists [11-13], and reasonable estimates of the interfacial energies of the competing phases can be made using broken-bond models [14], allowing a comparison of the competition in phase formation with the predictions of CNT. This comparison has been made by Styles et al. [10] and the temperature dependence of the CNT nucleation barrier (ΔG^*) for each thermodynamically permissible phase is shown in Fig. 1b. At ~180 °C, CNT predicts that the Al₁₉Ni₅Y₃ phase has the lowest barrier (Fig. 1b) and should form first. If for some reason that phase was constrained, the next most likely phase should be Al₉Ni₂. FCC Al is the 3rd most favored phase according to CNT, even though experimentally it dominates the initial crystallization reaction (Fig. 1a). Styles et al. compared such predictions for five different metallic glass compositions in the Al-Ni-Y system (showing a range of different first forming phases) and in only one case, did CNT correctly predict the first phase to form. Even qualitatively, CNT does not work very well for solid-state nucleation processes.

CNT was originally derived for the formation of spherical liquid droplets from a vapor without a change in composition [3]. It has been adapted for use in solid-state nucleation [1-3], and some authors have coupled the stochastic fluctuations to long range diffusion to try and account for the change in composition that occurs in many solid-state nucleation events [3]. However, the assumptions underlying the derivation of the most common form of the CNT rate equation are very strong, and one of the most important is the assumption that all thermally-induced stochastic fluctuations are possible, no matter how far their compositions lie from the bulk alloy composition [3]. This assumes that there always exists clusters with the correct chemistries and structures in the matrix, and the nucleation event occurs when a thermally-induced stochastic fluctuation brings a suitable one of them over the critical size (R*) for nucleation. The most commonly used CNT rate equation in solid-state phase transformations [1] does not consider the kinetics of formation of these clusters. This can be illustrated by the Gibbs energy curves shown in Fig. 2a. Consider a matrix with composition C_b at a temperature T₁. According to CNT, clusters with the compositions indicated by the red dots always exist in the matrix, and the driving forces for the nucleation of phases P1-P3 are represented by the magnitudes DF1-DF3. Note that the construction shown in Fig. 2a suggests that the largest driving force for nucleation (DF3) exists for the phase (P3) with a composition furthest from the bulk alloy composition (C_b). Experimentally, such phases are rarely seen to nucleate first, and



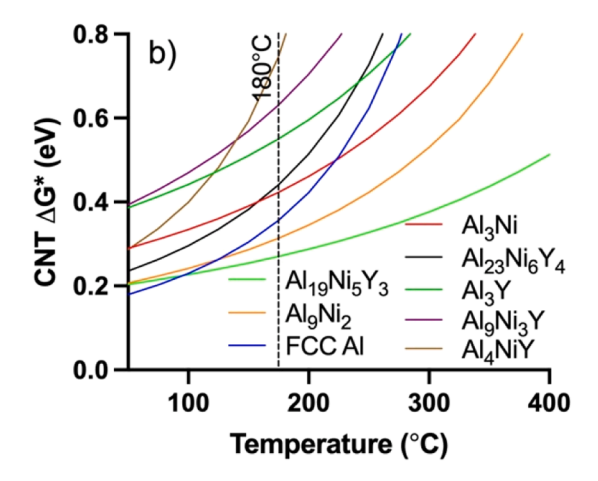


Fig. 1. a) Evolution of the phase fraction of different crystalline phases forming from an Al-9Ni-4Y metallic glasses heated at 10 °C/min in a synchrotron beam (experimental data replotted from Ref [10]), b) Calculated critical barrier to nucleation from CNT, ΔG^* , as a function of temperature for the thermodynamically permissible phases in an Al-9Ni-4Y metallic glass [10].

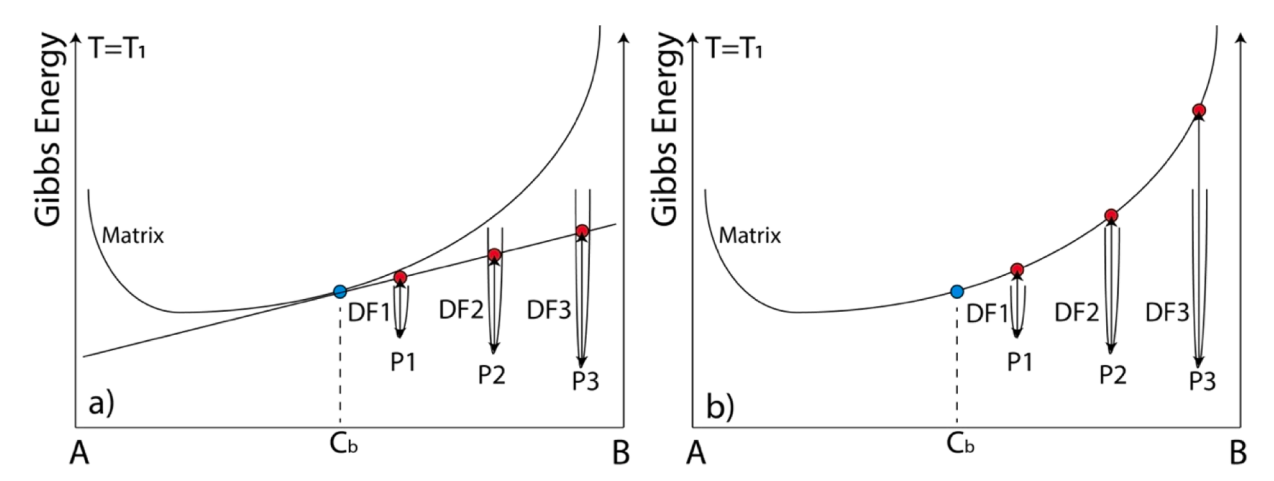


Fig. 2. Schematic Gibbs energy curves for a matrix and three precipitate phases (P1-P3) at a temperature of $T=T_1$. a) quantification of the onset driving force for nucleation (DF1-DF3) of each phase from a matrix composition C_b using the tangent construction. The red dots represent the compositions of stochastic clusters formed in the matrix in the context of CNT, b) an alternative quantification of the driving force for nucleation (DF1-DF3) of each phase from a matrix composition C_b assuming the cluster chemistries indicated by the red dots are long-lived geometric clusters instead of stochastically formed clusters.

rather the phase that nucleates first is usually the one with the composition closest to the matrix composition subject to the existence of a thermodynamic driving force and a reasonable interfacial energy.

Thermally-induced stochastic clusters that may evolve into nuclei of a new phase require atomic mobility. Whether the assumption that all thermally-induced stochastic clusters are possible is a good assumption will depend on a comparison of the time it takes for stochastic clusters to form, with the characteristic time for a nucleation event. Let us define a characteristic time for both processes: t_c being the characteristic time for stochastic clusters to form (which will be a strong function of the atomic mobility under the conditions considered), and tn being the characteristic time for a nucleation event. If t_n>>t_c, one might expect the assumption that all thermally-induced stochastic clusters are possible to be a reasonable approximation. This is shown at the right end of the timeline in Fig. 3. Under such conditions, one might expect the CNT framework to work reasonably well. These conditions will correspond to small driving forces (slow nucleation), systems with high mobility such as gases and liquids (fast stochastic cluster formation), and cases where the nucleating phase occurs without a change in chemistry.

However, in solid-state phase transformations we are often interested in nucleation of phases that exhibit a significant change in chemistry compared to the matrix, forming at relatively low temperatures where atomic mobility is limited, and where the nucleation rate is still high (giving a high number density of new phases). It is exactly these conditions that allow us to generate the nanostructures that deliver interesting properties to our materials for practical applications. In many cases of solid-state nucleation we are probably located closer to the left end of the timeline in Fig. 3 where the characteristic time for stochastic cluster formation is long compared to the nucleation time, $t_{\rm n}/t_{\rm c}{<<}1$. Under such conditions, it is difficult to imagine how clusters with

chemistries that lie far from the bulk alloy chemistry could form in the matrix by stochastic fluctuations. From this perspective, it may not be surprising that CNT does not work well for solid-state nucleation (not even qualitatively for predicting the competition in phase formation, Fig. 1).

This contribution presents a new model for nucleation (Section 2), applicable to systems where atomic mobility is limited, such as solid-state nucleation in engineering alloys at low temperature, although one may also find it interesting to apply to ceramics or inorganic glasses. It is a description designed to complement (and not replace) CNT. It is a nucleation description designed to apply at the left end of the timeline in Fig. 3, whereas CNT can be thought to be more appropriate at the right end of the timeline in Fig. 3. The connection between these two descriptions will be briefly discussed in Section 4.

2. A new model for solid-state nucleation based on geometric clusters

In systems where atomic mobility is limited, such as engineering alloys at low temperature, or metallic glasses undergoing devitrification, solid-state nucleation can still occur quicky. Under such conditions, the time to form thermally-induced stochastic clusters with the composition of the nucleating phases, is probably large compared to the characteristic time for nucleation (ie. $t_{\rm n}/t_{\rm c}{<}1$, Fig. 3). In this case, it is difficult to accept that nucleation is due to the formation of thermally-induced stochastic cluster formation in the framework of CNT.

If the local sites in a matrix with the correct chemistry for nucleation to occur do not form from stochastic fluctuations, then the alternative is that they must have already been there.

The approach to nucleation outlined below simply asks: what is the

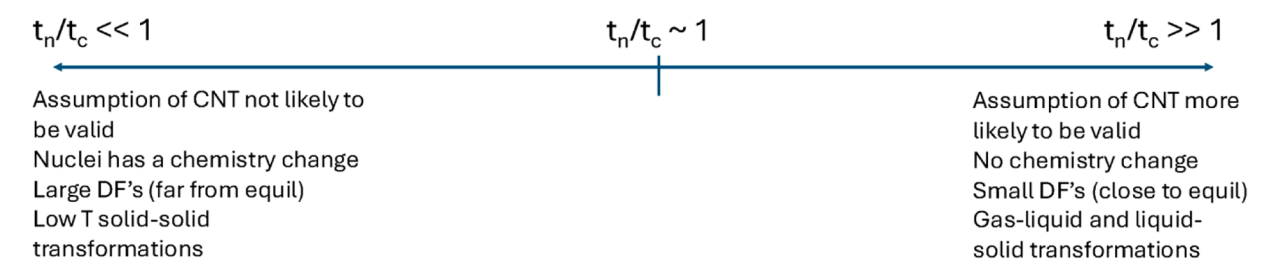


Fig. 3. Schematic timeline expressed in terms of the ratio of the characteristic time for thermally-induced stochastic clusters to form, t_c , and the characteristic time for a nucleation event to occur, t_n . Under conditions where $t_n/t_c >> 1$, the assumption that all thermally-induced stochastic clusters are possible which underlies CNT may be a good approximation. When $t_n/t_c << 1$, this assumption must break down.

probability of finding a nuclei-sized volume in a solid solution that has the chemistry corresponding to one of the thermodynamically permissible phases? Such regions are referred to as 'geometric clusters' since they are a statistical feature of the atomic configuration of a solid solution and not a result of stochastic fluctuations. Even in a random solid solution, the chemical composition is not uniform at the length scale of the nuclei. This has been shown previously in numerical simulations and the geometric clusters emphasised here likely correspond to the heterogeneities identified in numerical simulations by Spowart et al. [9].

To calculate the probability of finding a nuclei-sized volume in a solid solution with the chemistry corresponding to one of the thermodynamically permissible phases, consider a simplified A-B system quenched from high temperature so the atomic configuration of B in A may be well approximated as random. In this first treatment, we assume all species and phases have the same molar volume and we do not consider defect effects (e.g. surfaces, dislocations) on nucleation. The concentration of B atoms in the A-B alloy is C_b (#B atoms per unit volume) and we assume the nuclei is spherical with radius, \widetilde{R} .

We define two characteristic parameters, λ and ϕ :

$$\lambda = C_b \frac{4}{3} \pi \tilde{R}^3 \tag{1}$$

$$\phi = C_b \frac{4}{3} \pi \tilde{R}^3 k = \lambda k \tag{2}$$

 λ has units of #B atoms and it represents the *average* number of B atoms found in a matrix volume equivalent to the nuclei volume. λ is a measure of the bulk alloy composition.

 φ is the number of B atoms in the nuclei. It must be an integer and may be larger (solute rich nuclei) or smaller than λ (solute poor nuclei). k is a measure of the deviation of the nuclei chemistry from the bulk chemistry. If $k{=}1$, then the nuclei has the same composition as the bulk. If $k{<}1$, the nuclei is solute poor, if $k{>}1$, the nuclei is solute rich.

The number of potential nuclei per unit volume, N_{ν}^{p} , is the number of nuclei sized regions per unit volume multiplied by the probability, P, of a region having the chemistry (ϕ_{i}) of one of the permissible precipitate phases, i:

$$N_{\nu}^{p} = \frac{3}{4\pi\widetilde{p}^{3}} \cdot P = \frac{C_{b}}{\lambda} \cdot P$$
 (3)

P is the probability of finding a volume $\frac{4}{3}\pi\widetilde{R}^3$ containing φB atoms in the random solid solution.

For a random solution, P is defined by a discrete Poisson distribution, (Eq. (4)). A Poisson distribution describes the probability of a particular event occurring (ϕ) when we know the average frequency of events (λ), and those events are independent of each other. In our case, the event we are interested in is finding a nuclei sized volume containing the number of B atoms (ϕ_i) corresponding to the composition of one of the permissible phases, i. We know the average number of B atoms found in a nuclei-sized volume (λ) since this is defined by the bulk alloy composition.

$$P = \frac{\lambda^{\phi} exp(-\lambda)}{\phi!} \tag{4}$$

In Eq. (4), φ must be an integer: 0, 1, 2, 3.... since φ represents the number of B atoms in a nuclei.

Using Stirling's approximation, and after rearrangement, we obtain Eq. (5) for P and substituting into Eq. (3), we obtain an expression for the potential number of nuclei, N_p^p , Eq. (6).

$$P = \frac{\exp(-\lambda \alpha)}{\sqrt{2\pi \lambda k}} \text{ for } \lambda k \text{ taking on positive integer values 1, 2, 3...}$$
 (5)

$$N_{\nu}^{p} = \frac{C_{b}}{\lambda} \frac{exp(-\lambda \alpha)}{\sqrt{2\pi \lambda k}} \tag{6}$$

where α is a dimensionless parameter associated with the nuclei chemistry; $\alpha = 1 - k + k lnk$.

Because of the use of Stirling's approximation, Eq. (6) is valid only for $\varphi=\lambda k=1,\,2,\,3....$ i.e. it is not valid for $\varphi=0$, which would correspond to a nucleus containing no solute. However, the $\varphi=0$ case is straightforward since 0!=1, and for $\varphi=0$ to be true, k=0 which means no solute in the nucleus. For the $\varphi=0$ case, Eq. (4) reduces to a simple form and when combined with Eq. (3) we arrive at Eq. (7).

$$N_{\nu}^{p} = \frac{C_{b}}{\lambda} \cdot \exp(-\lambda)$$
 for $\phi = 0$, or equivalently $k = 0$ (7)

Eqs. (6) and (7) describe the number of potential nucleation sites based on the probability of finding nuclei sized volumes $(\frac{4}{3}\pi \widetilde{R}^3)$ with certain chemistries (ϕ_i) in a random solid solution.

Eq. (7) (for a nuclei containing no solute) has obviously the expected behaviour: for a given bulk alloy composition (C_b), as \widetilde{R} increases (λ increases (Eq. (1))) there are fewer sites corresponding to nuclei sized volumes with no B atoms. Similarly, for a given \widetilde{R} , as the bulk solute content (C_b) increases (λ increases) there are fewer sites corresponding to nuclei sized volumes with no B atoms. The behaviour of Eq. (6) is less obvious. Fig. 4a shows a plot of the potential number of nucleation sites calculated using Eqs. (6) and (7), as a function of φ , in a series of hypothetical A-xB alloys. A molar volume of 1×10^{-5} (m³/mol) has been used and a \widetilde{R} of 5×10^{-10} m is assumed for the purposes of calculations (corresponding to a nucleus containing 32 atoms).

Two important trends can be observed in Fig. 4a: a) the number of potential nucleation sites decreases as the solute content of the precipitate (ϕ) deviates from the bulk alloy composition, and b) the number of nucleation sites for a given precipitate chemistry (e.g. $\phi=8$, corresponding to A₃B) is higher in the alloy with a bulk solute content closer to the precipitate composition. Both of these trends show the expected behaviour.

It is also interesting to look at the quantitative numbers of potential nucleation sites for these hypothetical A-xB alloys which use physically reasonable input parameters. Consider a precipitate of composition A_3B . Fig. 4b shows the number of potential nucleation sites in the different hypothetical A-xB alloys as a function of the nuclei radius. For a nuclei radius of 5×10^{-10} m (corresponding to 32 atoms), alloys such as A-0.05B will contain 10^{23} – 10^{24} nuclei-sized volumes with a composition of A_3B (corresponding to φ =8B atoms) in the random solid solution. This corresponds to the order of magnitude of precipitates seen in many engineering alloys, e.g. [15,16].

 N_{ν}^{p} (Eqs. (6) and (7)) is the potential number of nuclei with a certain size (\widetilde{R}) and chemistry (ϕ). The geometric clusters with a suitable chemistry still need to change crystal structure and create an interface for a nucleation event to occur (we refer to such a process as 'activation'). There must be a driving force to pay for this interface formation but this driving force is not the traditional driving force calculated in CNT using the tangent construction (Fig. 2a). Since the geometric clusters that represent the potential nucleation sites are long-lived compared to thermally-induced stochastic fluctuations, we instead calculate the driving force as the difference between the Gibbs energy of the matrix phase at the composition of the precipitate, G^{m} , and the Gibbs energy of the precipitate at its nuclei composition, G^{p} (Fig. 2b).

The number of potential nuclei that are 'activated', N, might then be written as:

$$N = N_{v}^{p} \cdot exp\left(\frac{-\Delta \widetilde{G}}{kT}\right) \text{ where } \Delta \widetilde{G} \propto \frac{\gamma^{3}}{\left(G^{m} - G^{p}\right)^{2}}$$
 (8)

N can then be expressed as:

$$N = \frac{C_b}{\lambda} \cdot exp(-\lambda) \cdot exp\left(\frac{-\Delta \widetilde{G}}{kT}\right)$$
 for $\phi = 0$, or equivalently $k = 0$ (9)

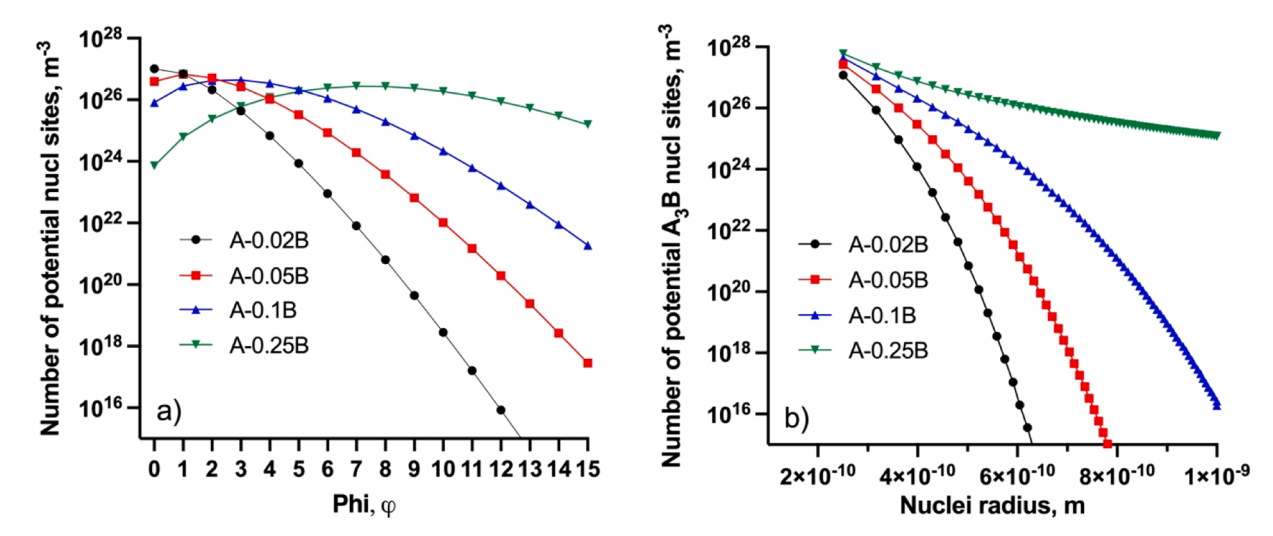


Fig. 4. a) Number of potential nucleation sites as a function of φ for A-0.02B, A-0.05B, A-0.1B and A-0.25B A nuclei radius \tilde{R} of 5×10^{-10} m and a molar volume of 1×10^{-5} m³/mol has been used for the calculations (corresponding to a nucleus containing 32 atoms), b) Number of potential nucleation sites as a function of nuclei radius for the same A-B alloys assuming a precipitate composition of A₃B.

$$N = \frac{C_b}{\lambda} \frac{exp(-\lambda \alpha)}{\sqrt{2\pi \lambda k}} \cdot exp\left(\frac{-\Delta \widetilde{G}}{kT}\right) \text{ for } \phi$$

$$= \lambda k \text{ taking on integer values 1, 2, 3...}$$
 (10)

The effect of the barrier $(exp\left(\frac{-\Delta\widetilde{G}}{kT}\right))$ on the number of activated nucleation sites depends on the size of the nuclei. In CNT, the critical nuclei size is defined as $\frac{2\gamma}{DF}$ (where DF is the onset driving force for nucleation shown in Fig. 2a) since the clusters grow by stochastic fluctuations and $\frac{2\gamma}{DF}$ is the smallest size from which they could survive and grow.

In the new approach proposed here, the regions corresponding to potential nuclei already exist in the matrix as geometric clusters with the chemistry corresponding to one of the thermodynamically permissible phases. They do not necessarily need to grow to pass some critical size, they just need to create an interface and change crystal structure (i.e. be 'activated'). They obviously must be equal to or greater in size than $\frac{2\gamma}{\mathrm{DF}}$ (where DF is defined as shown in Fig. 2b), otherwise once they have been activated they could not grow due to capillarity effects, but we may expect that the nuclei size which is first activated is the size that allows

the fastest nucleation.

Consider the Gibbs energy change on forming a nucleus of composition A_3B in the A-B system as a function of nucleus size in Fig. 5a. In this example, a driving force of $7.10^8~J/m^3$ (corresponding to 7000~J/mol for a molar volume of $1\times10^{-5}~m^3/mol$) and an interfacial energy, γ , of $0.15~J/m^2$ is used. A cluster containing only 1 B atom is indicated in Fig. 5a by $\varphi{=}1$. The smallest cluster that could be activated and survive to grow is indicated by $\varphi{=}5$ and contains 5 B atoms (and 20 atoms in total). This corresponds to a size close to $\frac{2\gamma}{DF}$. A nucleus of this size has a barrier of $\sim 0.72eV$ in this example. Also highlighted in Fig. 5a is a cluster containing 17 B atoms ($\varphi{=}17$, and 68 atoms in total). This cluster corresponds to a size close to $\frac{3\gamma}{DF}$ and such a cluster would not experience an energetic barrier to formation of an interface.

The effect of the potential barrier to creating an interface $(exp\left(\frac{-\Delta \widetilde{G}}{kT}\right))$ on the number of activated nuclei (Eq. (10)) is shown in Fig. 5b for the different A-xB alloys. A nuclei of composition A₃B is again assumed and the driving force and interfacial energy used in Fig. 5a is used. Fig. 5b indicates that in most cases the nuclei size that provides the largest number of activated sites (and hence the fastest nucleation)

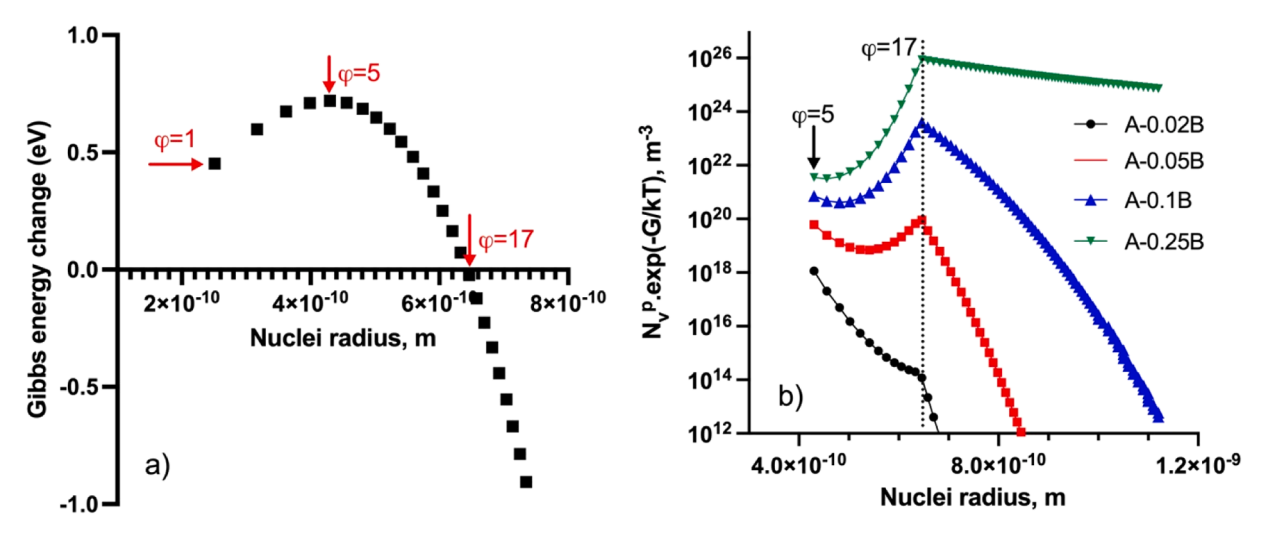


Fig. 5. a) Gibbs energy change as a function of nuclei size for a precipitate of composition A_3B forming in a hypothetical A-B alloy with a nucleation driving force of DF = 7.10^8 J/m³ and an interfacial energy, $\gamma = 0.15$ J/m², b) number of activated nucleation sites (Eq. (10)) of composition A_3B in a series of A-xB alloys as a function of nuclei size using the thermodynamic parameters in a).

corresponds to a size of $\sim \frac{3\gamma}{\Delta G}$ (R = 0.65nm) and contains 17 B atoms (and 68 atoms in total) in this example.

Eqs. (9) and (10) contain no kinetics. Changing crystal structure and creating an interface does require atoms to move. One approximation might be to assume that the atomic motion required is similar to that which would be required for atoms to jump across the interface, $\beta^* = \frac{\widehat{R}^2 D}{a^4}$ [1], where D is the solute diffusivity in the matrix at the temperature of interest and a is the lattice parameter.

We would then obtain for the nucleation rates:

$$\frac{dN}{dt} = \frac{\widetilde{R}^2 D}{\alpha^4} \frac{C_b}{\lambda} \cdot exp(-\lambda) \cdot exp\left(\frac{-\Delta \widetilde{G}}{kT}\right) \text{ for } \phi = 0, \text{ or equivalently } k = 0$$
(11)

compositions considered by Styles et al. are listed in the first column of Table 1. They include variations in both Ni and Y bulk contents. The first phase experimentally observed to form, and the temperature at which it forms, is listed in the 2nd column, as well as an estimate of the peak number density of particles of the first phase formed (calculated from the volume fraction and estimates of particles sizes from quantitative XRD).

There are advantages and disadvantages to using this metallic glass system to test the predictions of the nucleation model outlined in Section 2. The big advantage is that the system shows a competition in phase formation during crystallization which changes across the different glass compositions (Table 1). In some glass compositions the FCC Al appears first and in other compositions the Al₉Ni₂, or Al₁₉Ni₅Y₃ appear first. A model for nucleation should be able to predict this change in the competition in phase formation. An additional (simplifying) advantage is that the phases that appear during crystallization are mostly inter-

$$\frac{dN}{dt} = \frac{\widetilde{R}^2 D}{a^4} \frac{C_b}{\lambda} \frac{exp(-\lambda \alpha)}{\sqrt{2\pi \lambda k}} \cdot exp\left(\frac{-\Delta \widetilde{G}}{kT}\right) \text{ for } \phi = \lambda k \text{ taking on integer values 1, 2, 3...}$$
 (12)

Eqs. (11) and (12) obviously show the expected C-shape behaviour, reflecting the competition between thermodynamic and kinetics with temperature.

The above approach to solid-state nucleation is based on a random solution. It would give rise to a homogeneous distribution of precipitates, although this is not homogeneous nucleation in the spirit of CNT. Rather it is a reflection of the fact that in a random solution, the geometric clusters giving rise to the nucleation events are randomly distributed.

3. Comparison with experimental observations

To test the predictions of the geometric cluster nucleation model we consider two sets of experiments. In Section 3.1 we examine the competition in phase formation during the crystallization of Al-Ni-Y metallic glasses of different compositions [10]. In Section 3.2, we consider solvent trapping in Cu-Co [17,18] and Fe-Cu [19,20], which is predicted by the new nucleation model but which cannot be easily explained by CNT.

3.1. Competition in phase formation in Al-Ni-Y metallic glasses

Styles et al. [10] performed a series of in-situ synchrotron XRD experiments where they monitored the crystallization of different Al-Ni-Y metallic glasses during heating at $10~^{\circ}$ C/min. An example of the quantification of crystallization in Al-9Ni-4Y was shown in Fig. 1. In that case FCC Al was the first phase to form at \sim 180 $^{\circ}$ C. The five glass

metallic phases showing little compositional deviation from their stoichiometry. We will treat them as stoichiometric compounds. Even for the FCC Al phase which forms first in two of the glass compositions (Table 1), lattice parameter measurements suggests that it is almost pure Al with little solvent trapping [10]. We treat it as pure Al in the following calculations. Solvent trapping during nucleation is addressed in Section $\frac{3}{2}$

An amorphous matrix also means that more reasonable estimates of the interfacial energies of the nucleating phases can be made considering only the chemical contribution (using broken-bond models [14] as done by Styles et al. [10]). Two independent CALPHAD thermodynamic descriptions of the Al-Ni-Y system also exist (Golumbfskie et al. [11–12] and Huang et al. [13]) and the different descriptions show good agreement for the phases that are in common which provides some confidence

Table 2Interfacial energy between the precipitating phases and the metallic glass matrix, calculated by Styles et al. [10] using the broken-bond model.

| Nucleating phase | Interfacial energy (J/m²) |
|---|---------------------------|
| FCC Al | 0.08 |
| Al ₉ Ni ₂ | 0.11 |
| Al ₃ Ni | 0.20 |
| Al ₃ Y | 0.27 |
| $Al_{19}Ni_5Y_3$ | 0.17 |
| Al ₂₃ Ni ₆ Y ₄ | 0.12 |
| Al_9Ni_3Y | 0.14 |

Table 1
Comparison of experimental observations [10] and calculations (CNT and geometric cluster model) of the first phase to form during heating of a series of Al-Ni-Y metallic glasses.

| Alloy (at. %) | Experimentally observed 1st phase (T), estimated $N_{\rm v}$ [10] | CNT predicted 1st phase (and 2nd most likely) phase at crystallization T | New model prediction of 1st phase at crystallization temperature, N, (Eq. (9) or (10)) |
|-----------------------------|---|--|--|
| Al-9Ni-4Y Al-10Ni- 4Y | FCC Al (180 °C), 4×10^{23} m ⁻³ FCC Al (218 °C), 9×10^{22} m ⁻³ | $\begin{array}{l} Al_{19}Ni_{5}Y_{3}\;(Al_{9}Ni_{2})\\ Al_{19}Ni_{5}Y_{3}\;(Al_{9}Ni_{2}) \end{array}$ | FCC Al, $2.48 \times 10^{26} \text{ m}^{-3}$ FCC Al, $7.36 \times 10^{25} \text{ m}^{-3}$ |
| Al-13Ni- 4Y | Al_9Ni_2 (270 °C), $9 \times 10^{23} \text{ m}^{-3}$ | $Al_{19}Ni_5Y_3$ (Al_9Ni_2) | Al_9Ni_2 , $3.55 \times 10^{25} m^{-3}$ |
| Al-15Ni- 4Y | Al ₉ Ni ₂ & Al ₃ Ni (300 °C), both 5×10^{23} m ⁻³ | $Al_{19}Ni_5Y_3$ (Al_9Ni_2) | Al ₃ Ni, 4.87×10^{25} m ⁻³ Al ₉ Ni ₂ , 2.80×10^{25} m ⁻³ |
| Al-15Ni- 10Y | Al ₁₉ Ni ₅ Y ₃ (376C), - | $Al_{19}Ni_{5}Y_{3}$ ($Al_{23}Ni_{6}Y_{4}$) | $Al_{19}Ni_5Y_3$, $8.13\times10^{25}~m^{-3}$ |

in the descriptions. For the following calculations, we use the thermodynamic description provided by Golumbfskie et al. [11–12] but we make two modifications. Firstly, we include the thermodynamic description of the Al_9Ni_3Y phase which was included in Golumbfskie's PhD thesis [11] (also used by Styles et al. [10]) but not in the published article [12]. Secondly, we make a change to the thermodynamic description of the Al_9Ni_2 phase. Golumbfskie et al. artificially added energy to the Al_9Ni_2 phase in their description to deliberately destabilise it at high temperature [12]. Unfortunately, the intermetallic Al_9Ni_2 phase does not exist in the Huang et al. [13] description but it is included in the ThermoCalc TCAL5 database. We have manually adjusted the description of this stoichiometric Al_9Ni_2 to match the Gibbs energy as a function of temperature in the TCAL5 database, so as to avoid the artificial destabilising imposed by Golumbfskie et al. [12]. The interfacial energies used for each phase are taken from [10] and listed in Table 2.

The disadvantage of using a metallic glass system to test the predictions of the nucleation model outlined in Section 2 is that we do not have a thermodynamic description for the glass matrix. We use the Gibbs energy of the supercooled liquid as an estimate for the glassy matrix but they are not exactly the same. This will lead to an overestimation of the driving forces for nucleation but we expect this to be systematic and not favour one nucleating phase over another. This means we assume that the statistical geometric fluctuations in the glass are the same as those in the liquid. As a result, we emphasise a comparison of the experimental and predicted first phase formed during crystallization, rather than the absolute number densities of particles.

We expect the phase to nucleate first during crystallization to be the phase with the highest nucleation rate at the temperature of crystallization. We will use Eqs. (9) and (10), describing the expected number of activated nucleation sites, to test predictions of which phase should form first according to the geometric cluster nucleation model. The new nucleation model was presented as a binary A-B system. To apply this to a ternary A-B-C system, such as Al-Ni-Y, we must calculate the probability of finding nuclei-sized volumes with the Ni and Y chemistries corresponding to one of the thermodynamically permissible phases. As a first approximation, we assume the Ni and Y are both randomly distributed in the matrix with no correlation (ie. short range ordering (SRO) does not exist). The probability can then be calculated as the product of the probability a volume will have the correct Ni chemistry (P_{Ni}) and the probability it will have the correct Y chemistry (P_Y). The calculations for the geometric cluster model are summarised in Tables 3 to 7. Each Table corresponds to one of the Al-Ni-Y compositions and the calculations apply at the temperature of crystallization observed experimentally.

Consider the Al-9Ni-4Y alloy as an example (Table 3). As shown in Fig. 1a, this glass starts to crystallise at 180 °C and the first phase to form is the FCC Al. The seven most likely phases to form are listed in column 1 of Table 3. The nucleation driving force (DF) for each phase to form at 180 °C is defined as shown in Fig. 2b and listed in the 2nd column. Using the interfacial energies (Table 2), a *first estimate* of the nuclei radius is calculated as $3\gamma/DF$ (column 3). The corresponding numbers of Ni and Y atoms in the nuclei from this first estimate of the nuclei size are listed as ϕ_{Ni} (column 4) and ϕ_{Y} (column 5). We model the FCC Al as pure Al so the nuclei contains no Ni or Y atoms. However, the other phases do contain

Ni and/or Y atoms, but the number of Ni and Y atoms are not necessarily integer values in the ϕ_{Ni} and ϕ_{Y} columns of Table 3 as they must be. The closest values of φ_{Ni} and φ_{Y} that are integer values and respect the stoichiometry of each phase are listed as ϕ_{Ni}^{Mod} and ϕ_{Y}^{Mod} (columns 6 and 7) and these values define the most suitable choice for the nuclei radius, \widetilde{R} (column 8). As can be seen from Table 3, typical nuclei sizes are 10–30 atoms in total and lie between 3-5Å. The probability of finding a nucleisized volume in the matrix with the Ni or Y composition of the relevant phase is then listed as P_{Ni} or P_Y (columns 10 and 11). These probabilities show interesting behaviours and capture the essence of the geometric cluster nucleation model. The values of these probabilities are a combination of how far away the Ni or Y composition of the phase is from the bulk alloy content as well as the size of the nuclei. Consider the FCC Al and the Al₃Y phases in Table 3. Both of these phases contain no Ni, but the probability of finding a Ni-free volume with the size of the FCC Al nuclei is 17.4%, whereas for the Al₃Y, it is 48.7%. This large difference is entirely because the nuclei volume of the Al₃Y phase is much smaller than the FCC Al in this example (8 atoms vs 20 atoms, column 9). The comparison between FCC Al and Al₃Ni in Table 3 is also interesting. In this case, their nuclei sizes are closer (20 atoms for the FCC Al vs 16 atoms for the Al₃Ni) and both have Ni contents that deviate significantly from the 9% present in the alloy. The FCC Al has a Ni content that deviates from the bulk by -9%, whereas the Al₃Ni has a Ni content that deviates from the bulk by +16%. As shown in Fig. 4a, as the composition of the nuclei deviates further and further from the bulk composition, the numbers of volumes with a suitable chemistry decreases. This is the reason why the probability of finding an Al₃Ni nuclei-sized volume with 25% Ni is 4x smaller than the probability of finding an FCC Al nucleisized volume with no Ni, in this alloy composition. Since this is a ternary alloy, the probability of finding a suitable nuclei volume with the correct Ni and Y chemistries is PNi x PY (column 12) (assuming random distributions for both Ni and Y and no correlation between the species) and from here the maximum expected number of nuclei, N, can be calculated for each phase. For the Al-9Ni-4Y alloy crystallizing at 180 °C, the largest number of nuclei corresponds to the FCC Al phase and this would be expected to be the first phase to form at this temperature according to the geometric cluster model. This agrees well with the experimental observations (Fig. 1 and Table 1).

Similar calculations have been made for each alloy composition (Tables 3 to 7). The phase with the largest number of nuclei (and hence faster rate) for each alloy composition is summarised in column 3 of Table 1. In each of the metallic glass compositions, the geometric cluster model correctly predicts the first phase to form experimentally. The predictions of CNT (made using plots such as that shown in Fig. 1b) are also summarised in Table 1. In only one case (Al-15Ni-10Y) does CNT provide a correct prediction of the first phase to form.

Whilst the geometric cluster model can predict well the competition of phase nucleation during crystallization in the different Al-Ni-Y glasses experimentally investigated by Styles et al. [10], the maximum number densities of particles predicted by the geometric cluster model are a factor of 100 higher than the numbers observed experimentally (Table 1). There are two reasons for this. The first is that we have estimated the Gibbs energy of the glassy matrix with the Gibbs energy of the supercooled liquid. This is known to lead to an overestimation of the

Table 3Calculations of the expected number of nuclei to form for the different phases in Al-9Ni-4Y at 453K (180C).

| Phase | DF (J/m ³) | 3γ/DF (Å) | ϕ_{Ni} | ϕ_Y | ϕ_{Ni}^{Mod} | ϕ_Y^{Mod} | $\widetilde{R}(A)$ | # atoms | P _{Ni} | P_{Y} | P _{Ni} x P _Y | N (#/m ³) |
|---|------------------------|-----------|-------------|----------|-------------------|----------------|--------------------|---------|-----------------|---------|----------------------------------|-----------------------|
| FCC Al | 5.64×10 ⁸ | 4.25 | 0 | 0 | 0 | 0 | 4.25 | 20 | 0.174 | 0.460 | 0.0799 | 2.48×10 ²⁶ |
| Al ₃ Ni | 1.50×10^{9} | 3.99 | 4 | 0 | 4 | 0 | 3.99 | 16 | 0.043 | 0.527 | 0.0228 | 8.60×10^{25} |
| Al ₉ Ni ₂ | 7.32×10^{8} | 4.51 | 4.20 | 0 | 6 | 0 | 5.08 | 33 | 0.050 | 0.267 | 0.0132 | 2.42×10^{25} |
| $Al_{19}Ni_5Y_3$ | 1.59×10^{9} | 3.22 | 1.55 | 0.93 | 5 | 3 | 4.75 | 27 | 0.063 | 0.073 | 0.0046 | 1.03×10^{25} |
| Al ₂₃ Ni ₆ Y ₄ | 9.85×10^{8} | 3.65 | 2.24 | 1.49 | 6 | 4 | 5.08 | 33 | 0.050 | 0.035 | 0.0017 | 3.12×10^{24} |
| Al ₉ Ni ₃ Y | 1.00×10^{9} | 4.19 | 4.27 | 1.42 | 6 | 2 | 4.69 | 26 | 0.022 | 0.199 | 0.0044 | 1.03×10^{25} |
| Al ₃ Y | 2.62×10^{9} | 3.09 | 0 | 1.86 | 0 | 2 | 3.17 | 8 | 0.487 | 0.039 | 0.0188 | 1.46×10^{26} |

Table 4
Calculations of the expected number of nuclei to form for the different phases in Al-10Ni-4Y at 491K (218C).

| Phase | DF (J/m^3) | $3\gamma/DF$ (Å) | ϕ_{Ni} | ϕ_{Y} | ϕ_{Ni}^{Mod} | ϕ_Y^{Mod} | $\widetilde{R}(A)$ | # atoms | P_{Ni} | P_{Y} | $P_{Ni} \; x \; P_Y$ | $N (\#/m^3)$ |
|-----------------------------------|----------------------|------------------|-------------|------------|-------------------|----------------|--------------------|---------|----------|---------|----------------------|-----------------------|
| FCC Al | $5.19{	imes}10^{8}$ | 4.62 | 0 | 0 | 0 | 0 | 4.62 | 25 | 0.083 | 0.369 | 0.0305 | 7.36×10^{25} |
| Al ₃ Ni | 1.42×10^{9} | 4.21 | 4.72 | 0 | 5 | 0 | 4.29 | 20 | 0.037 | 0.449 | 0.0165 | 4.97×10^{25} |
| Al ₉ Ni ₂ | 6.86×10^{8} | 4.81 | 5.11 | 0 | 6 | 0 | 5.08 | 33 | 0.067 | 0.267 | 0.0179 | 3.27×10^{25} |
| $Al_{19}Ni_5Y_3$ | 1.53×10^{9} | 3.33 | 1.72 | 1.03 | 5 | 3 | 4.75 | 27 | 0.082 | 0.073 | 0.0060 | 1.34×10^{25} |
| $Al_{23}Ni_6Y_4$ | 9.23×10^{8} | 3.90 | 2.72 | 1.81 | 6 | 4 | 5.08 | 33 | 0.067 | 0.035 | 0.0023 | 4.22×10^{24} |
| Al ₉ Ni ₃ Y | 9.54×10^{8} | 4.40 | 4.97 | 1.66 | 6 | 2 | 4.69 | 26 | 0.032 | 0.199 | 0.0064 | 1.49×10^{25} |
| Al_3Y | 2.52×10^{9} | 3.21 | 0 | 2.09 | 0 | 3 | 3.62 | 12 | 0.301 | 0.012 | 0.0035 | 1.77×10^{25} |

Table 5Calculations of the expected number of nuclei to form for the different phases in Al-13Ni-4Y at 543K (270C).

| Phase | DF (J/m ³) | $3\gamma/DF$ (Å) | ϕ_{Ni} | $\phi_{ m Y}$ | ϕ_{Ni}^{Mod} | ϕ_Y^{Mod} | $\widetilde{R}(A)$ | # atoms | P_{Ni} | P_{Y} | $P_{Ni} \; x \; P_Y$ | $N (\#/m^3)$ |
|---|------------------------|------------------|-------------|---------------|-------------------|----------------|--------------------|---------|----------|---------|----------------------|-----------------------|
| FCC Al | 4.58×10 ⁸ | 5.24 | 0 | 0 | 0 | 0 | 5.24 | 36 | 0.009 | 0.233 | 0.0021 | 3.40×10^{24} |
| Al ₃ Ni | 1.31×10^{9} | 4.57 | 6.02 | 0 | 7 | 0 | 4.81 | 28 | 0.045 | 0.326 | 0.0146 | 3.13×10^{25} |
| Al ₉ Ni ₂ | 6.23×10^{8} | 5.30 | 6.83 | 0 | 7 | 0 | 5.34 | 39 | 0.106 | 0.214 | 0.0227 | 3.55×10^{25} |
| $Al_{19}Ni_5Y_3$ | 1.46×10^{9} | 3.49 | 1.99 | 1.19 | 5 | 3 | 4.75 | 27 | 0.135 | 0.073 | 0.0099 | 2.21×10^{25} |
| Al ₂₃ Ni ₆ Y ₄ | 8.38×10^{8} | 4.30 | 3.64 | 2.42 | 6 | 4 | 5.08 | 33 | 0.120 | 0.035 | 0.0042 | 7.58×10^{24} |
| Al ₉ Ni ₃ Y | 8.86×10^{8} | 4.74 | 6.20 | 2.07 | 9 | 3 | 5.37 | 39 | 0.039 | 0.137 | 0.0053 | 8.16×10^{24} |
| Al ₃ Y | 2.38×10^{9} | 3.40 | 0 | 2.48 | 0 | 3 | 3.62 | 12 | 0.210 | 0.012 | 0.0025 | 1.24×10^{25} |

Table 6Calculations of the expected number of nuclei to form for the different phases in Al-15Ni-4Y at 543K (300C).

| Phase | DF (J/m ³) | 3γ/DF (Å) | ϕ_{Ni} | ϕ_Y | ϕ_{Ni}^{Mod} | ϕ_Y^{Mod} | $\widetilde{R}(A)$ | # atoms | P_{Ni} | P _Y | P _{Ni} x P _Y | N (#/m ³) |
|-----------------------------------|------------------------|-----------|-------------|----------|-------------------|----------------|--------------------|---------|----------|----------------|----------------------------------|-----------------------|
| FCC Al | 3.72×10^{8} | 6.45 | 0 | 0 | 0 | 0 | 6.45 | 68 | 0.00004 | 0.0665 | 2.5×10^{-6} | 2.28×10^{21} |
| Al ₃ Ni | $1.25{	imes}10^{9}$ | 4.80 | 6.99 | 0 | 7 | 0 | 4.81 | 28 | 0.0694 | 0.3263 | 0.0227 | 4.87×10^{25} |
| Al ₉ Ni ₂ | 5.86×10^{8} | 5.63 | 7.88 | 0 | 8 | 0 | 5.63 | 45 | 0.1265 | 0.1652 | 0.0209 | 2.80×10^{25} |
| $Al_{19}Ni_5Y_3$ | 1.42×10^{9} | 3.59 | 2.17 | 1.30 | 5 | 3 | 4.75 | 27 | 0.1609 | 0.0733 | 0.0118 | 2.63×10^{25} |
| $Al_{23}Ni_6Y_4$ | 7.89×10^{8} | 4.56 | 4.36 | 2.91 | 6 | 4 | 5.08 | 33 | 0.1468 | 0.0345 | 0.0051 | 9.24×10^{24} |
| Al ₉ Ni ₃ Y | 8.47×10^{8} | 4.96 | 7.09 | 2.36 | 9 | 3 | 5.37 | 39 | 0.0643 | 0.1367 | 0.0088 | 1.36×10^{25} |
| Al_3Y | 2.30×10^{9} | 3.52 | 0 | 2.74 | 0 | 3 | 3.62 | 12 | 0.1653 | 0.0117 | 0.0019 | 9.73×10^{24} |

Table 7Calculations of the expected number of nuclei to form for the different phases in Al-15Ni-10Y at 648K (375C).

| Phase | DF (J/m ³) | 3γ/DF (Å) | ϕ_{Ni} | ϕ_Y | ϕ_{Ni}^{Mod} | ϕ_Y^{Mod} | $\widetilde{R}(A)$ | # atoms | P _{Ni} | P _Y | P _{Ni} x P _Y | N (#/m ³) |
|-----------------------------------|------------------------|-----------|-------------|----------|-------------------|----------------|--------------------|---------|---------------------|----------------------|----------------------------------|-----------------------|
| FCC Al | 2.89×10^{8} | 8.30 | 0 | 0 | 0 | 0 | 8.30 | 144 | 4×10^{-10} | 5×10^{-7} | 2.3×10^{-16} | 9.60×10^{10} |
| Al ₃ Ni | 1.09×10^{9} | 5.51 | 10.53 | 0 | 11 | 0 | 5.59 | 44 | 0.036 | 0.012 | 0.00044 | 5.97×10^{23} |
| Al_9Ni_2 | 4.95×10^{8} | 6.67 | 13.58 | 0 | 14 | 0 | 6.73 | 77 | 0.084 | 4.5×10^{-4} | 0.00004 | 2.96×10^{22} |
| $Al_{19}Ni_5Y_3$ | 1.31×10^{9} | 3.88 | 2.73 | 1.64 | 5 | 3 | 4.75 | 27 | 0.161 | 0.227 | 0.0365 | 8.13×10^{25} |
| $Al_{23}Ni_6Y_4$ | 6.66×10^{8} | 5.40 | 7.24 | 4.83 | 9 | 6 | 5.81 | 50 | 0.114 | 0.147 | 0.0167 | 2.03×10^{25} |
| Al ₉ Ni ₃ Y | 7.50×10^{8} | 5.60 | 10.24 | 3.41 | 12 | 4 | 5.91 | 52 | 0.044 | 0.172 | 0.0075 | 8.68×10^{24} |
| Al ₃ Y | 2.10×10^{9} | 3.85 | 0 | 3.60 | 0 | 4 | 3.99 | 16 | 0.091 | 0.056 | 0.0051 | 1.92×10^{25} |

nucleation driving force and leads to smaller nuclei and higher number densities. This is the reason why we have emphasised the comparative nucleation rates between phases in the context of the competition in nucleation, rather than absolute numbers. The second reason is the geometric cluster model describes the maximum number density (not all nuclei may survive). This needs to be coupled with growth and coarsening models into an integrated precipitation model to be able to compare quantitatively with experimental nucleation rates and maximum number densities.

3.2. Solvent trapping during solid-state nucleation

The example shown in Section 3.1 considered the competition in nucleation between a range of phases of fixed (stoichiometric) compositions. Most of the precipitating phases in the Al-Ni-Y system are intermetallics, and even the case of FCC Al appears to be close to pure Al in practice [10].

However, in situations where solution phases nucleate in the solid, experimental observations have reported substantial solvent trapping in

some cases. These reports of solvent trapping have mostly emerged since the advent of atom probe tomography (APT), which allows measurement of local chemistries at the nm scale. Setna et al. [17] report solvent trapping of 24% Cu in Co precipitates formed in a Cu-2Co alloy at short times at 450 °C. The Co precipitates at equilibrium are almost 100% pure Co. Cerezo et al. [18], also using APT, report solvent trapping of more than 10% Cu in small Co precipitates precipitated at temperatures around 500 °C. They report that Co precipitates with compositions of 100% Co are only observed during coarsening.

Morley et al. [19] studied the solvent trapping of Fe in Cu precipitates formed in dilute Fe-Cu alloys at low temperature. The Cu precipitates are almost 100% pure Cu under equilibrium conditions. Morley et al. also used APT for their measurements but specifically tried to account for the artifacts in APT measurements (aberrations in the trajectories of different ions) which was becoming better recognized as the field matured. Morley et al. claim that the amount of Fe solvent trapping depends on the temperature of Cu precipitation. At temperatures of $\sim\!330~^\circ\text{C}$, solvent Fe trapping of 17% is observed in the Cu precipitates. At 365 $^\circ\text{C}$, the Fe trapping is 14% and at 400 $^\circ\text{C}$, the

trapping is \sim 7%. However, not all agree with the claims of solvent trapping measured by APT. Shu et al. [20] used a combination of characterization tools (including SANS) to study the composition of Cu precipitates formed in a similarly dilute Fe-Cu alloy aged at low temperatures and subjected to neutron irradiation. They claim there is no significant solvent trapping in the Cu precipitates under these conditions, although care should be taken to generalize given the different experimental conditions.

To avoid potential artifacts associated with APT measurements of solvent trapping in very small solid-state precipitates, Orthacker et al. [21-22] used scanning transmission electron microscopy combined with electron tomography to examine the compositions of small L12 Al $_3$ (Sc, Zr) precipitates formed in Al-Sc-Zr alloys. Even though the L12 particles are usually assumed to be stoichiometric with respect to the Al content, these authors showed that significant Al solvent trapping is observed even in these compounds. They report an Al content of 88% instead of the expected 75%.

It appears that solvent trapping during solid state precipitation is real (and not simply an artifact of APT) and it is rather a question of accurate quantification of the amount of solvent trapping and how this may vary with different precipitation conditions. This solvent trapping is not easy to explain using CNT. Non-classical models for nucleation can rationalize nuclei compositions that deviate from equilibrium, e.g. Chapter 4 of [3], but they do not account for the large solvent trapping summarized above.

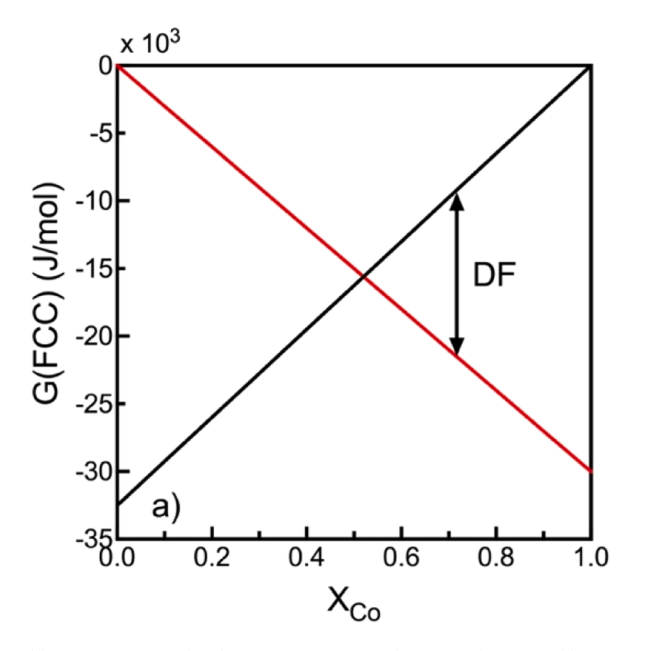
Solvent trapping is predicted by the geometric cluster nucleation model and in the following we use the dilute Cu-2Co (at. %) and Fe-2Cu (at. %) alloy systems as examples for illustration. The Gibbs energy curves for FCC Cu(Co) and Co(Cu) phases at 500 °C are shown in Fig. 6a. Instead of representing the Gibbs energy as a miscibility gap, we use separate Gibbs energy curves for each phase by extrapolating the Cu rich end of the curve (from ThermoCalc TCCu4 database) to the Co rich region for FCC Cu(Co), and the Co rich end of the curve to the Cu rich region for FCC Co(Cu). A similar formulation is shown in Fig. 6b for the Fe-Cu system at 500 °C for the BCC Fe(Cu) and BCC Cu(Fe) phases. For the cases shown in Fig. 6, the equilibrium composition of the precipitating phase is almost 100% pure Co in Cu (Fig. 6a), or pure Cu in Fe (Fig. 6b). However, if we consider dilute matrix compositions such as Cu-2Co or Fe-2Cu, there will exist within the matrix geometric clusters of different Co or Cu contents. In both systems, if those geometric

clusters contain more than 50% solute, then a driving force (DF) (defined as shown in Fig. 2b) exists for nucleation (Fig. 6).

Let us consider first the Cu-2Co system at 500 °C. One can appreciate from Fig. 6a that the nucleus size (assumed to be $3\gamma/DF$ for the purposes of this calculation) will be smaller for a nucleus with a composition of 100% Co, than one with a composition of 70% or 80% Co (since the driving force is larger). However, the number of geometric clusters with a composition of 100% Co in a random solid solution of Cu-2Co will be much smaller than the number with a composition of 70% or 80% Co. There are two competing effects – higher driving forces (for nuclei with compositions closer to 100% Co) mean smaller nuclei which means more potential sites. However, the probability of a potential site having the correct chemistry decreases as the chemistry deviates further and further from the bulk alloy chemistry (Fig. 4).

Calculations of the number of "activated" nuclei in an Cu-2Co alloy at 500 °C, as a function of the composition of the nuclei are shown in Fig. 7, for three different assumptions for the interfacial energy ($\gamma = 0.1$ J/m^2 in Fig. 7a, 0.15 J/m^2 in Fig. 7b and 0.2 J/m^2 in Fig. 7c). The best estimate for the interfacial energy of the Co precipitates in this system is 0.15 J/m^2 [23]. Consider Fig. 7a where it is assumed $\gamma = 0.1 \text{ J/m}^2$. The smallest, and most numerous nuclei are those containing three Co atoms $(\phi=3)$, corresponding to a nucleus composition of ~66% Co and a radii of \sim 2.3A. If one felt that such a nucleus size contained too few atoms to be physically reasonable, then the next most numerous choice of nuclei contains four Co atoms (ϕ =4), corresponding to a nucleus composition of \sim 65% Co and a radii of \sim 2.6A. For a nuclei containing five Co atoms (ϕ =5), the nucleus composition would be ~64% Co and a radii of \sim 2.8A. Regardless of the choice, for an interfacial energy of 0.1 J/m², the geometric cluster model would predict solvent trapping of around 35% at 500 $^{\circ}$ C in an alloy such as Co-2Co. The effect of different choices of the interfacial energy are shown in Fig. 7b and c. As the interfacial energy increases, the degree of predicted solvent trapping decreases, but for interfacial energies thought appropriate for Co precipitation in dilute Cu-Co (ie. $\sim 0.15 \text{ J/m}^2$ [23]), solvent trapping of $\sim 25\%$ is predicted $(\phi=3)$ and this is quantitatively similar to the values reported by Setna et al. [17]. Incidentally, the number of nuclei predicted in Fig. 7 for the Cu-2Co system at 500 $^{\circ}$ C is 10^{23} – 10^{24} m⁻³, which also corresponds well to the peak number densities observed experimentally in this alloy at this temperature [4].

Similar calculations are shown in Fig. 8 for the predicted



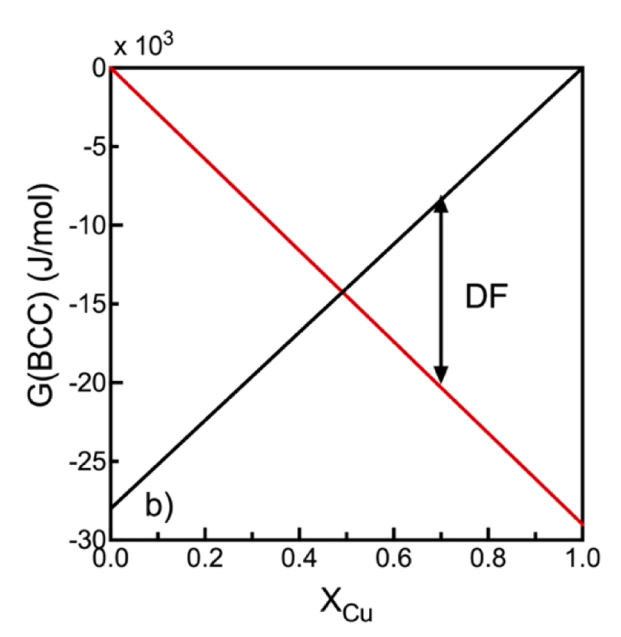


Fig. 6. Gibbs energy curves for the a) FCC Co(Cu) and Cu(Co) phases, and b) BCC Fe(Cu) and Cu(Fe) phases, at 500 °C. The Gibbs energy of the matrix phase is shown in black, and that of the precipitate phase is shown in red.

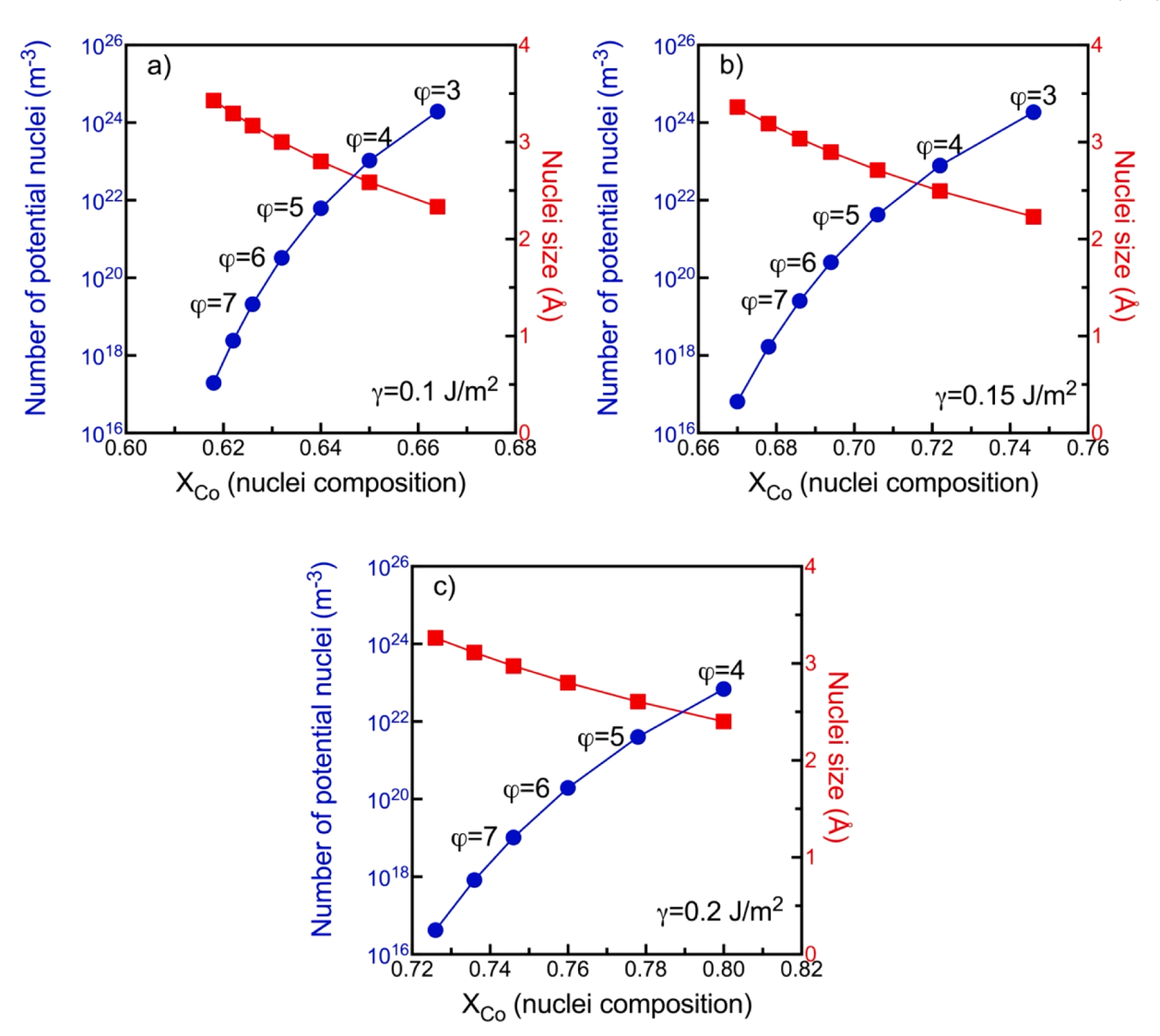


Fig. 7. Calculations of the predicted number of nuclei in the Cu-2Co system at 500 °C, as a function of nuclei composition, a) assuming $\gamma = 0.1 \text{ J/m}^2$, b) assuming $\gamma = 0.1 \text{ J/m}^2$, assuming $\gamma = 0.2 \text{ J/m}^2$.

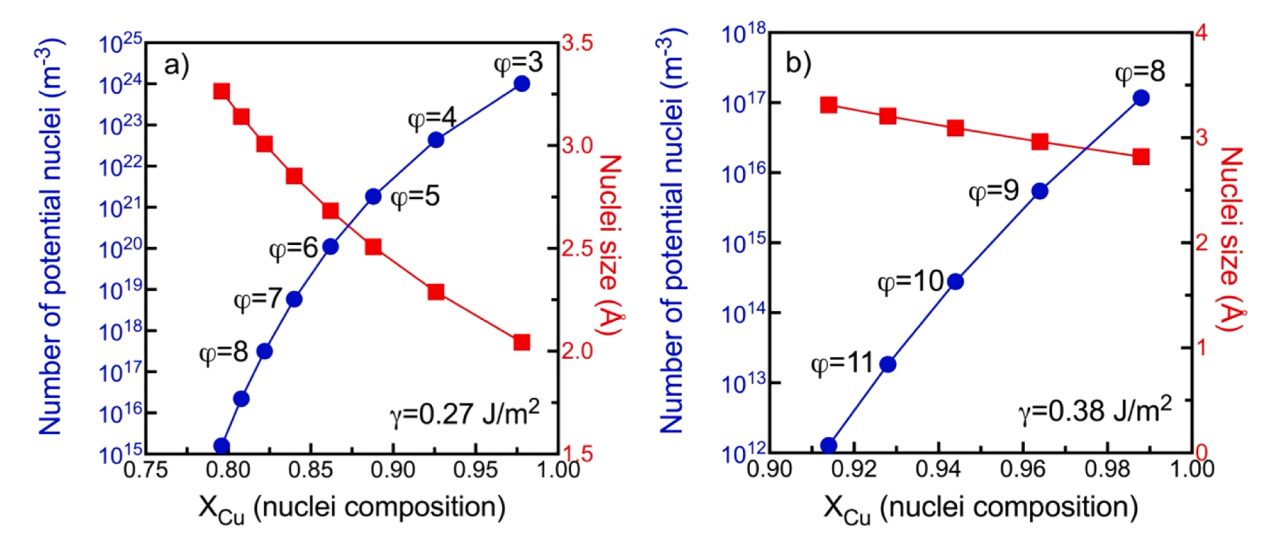


Fig. 8. Calculations of the predicted number of nuclei in the Fe-2Cu system at 500 °C, as a function of nuclei composition, a) assuming $\gamma = 0.27 \text{ J/m}^2$, b) assuming $\gamma = 0.38 \text{ J/m}^2$.

compositions of nuclei forming in Fe-2Cu alloys at 500 °C. Literature estimates of the interfacial energy of the BCC Cu precipitates in the Fe matrix range from 0.27-0.38 J/m² [24]. The effects of these values of the interfacial energies are shown in Fig. 8a and b. For an interfacial energy of 0.27 J/m² (Fig. 8a), the smallest nuclei according to the geometric cluster model contains three Cu atoms and would exhibit only $\sim 2-3\%$ solvent trapping at 500 °C. Nuclei containing 4 or 5 Cu atoms could exhibit trapping of $\sim 10\%$ Fe. The number density of nuclei predicted in this case (10²³–20²⁴ m⁻³) also agrees well with the number density observed experimentally in Fe-2Cu at temperatures close to 500 °C [25–26]. With a higher interfacial energy (0.38 J/m², Fig. 8b), the predicted level of solvent trapping is less than 2% Fe at 500 $^{\circ}$ C. As shown in Figs. 7 and 8, solvent trapping, at levels consistent with experimental reports, is a natural prediction of the geometric cluster model for nucleation, which also demonstrates good agreement for the predicted number of nuclei at 500 °C in these two alloys.

Many more measurements of the compositions of very small solidstate precipitates should be encouraged and understanding their dependence on temperature of formation and bulk alloy composition will provide an excellent test of the predictions of the geometric cluster model for nucleation.

4. Transition between a model based on geometric fluctuations and \mbox{CNT}

In the introduction, we used a timeline (Fig. 3) to discuss potential issues with the assumption that all possible clusters could form stochastically, no matter how far their compositions lie from the average matrix composition, when applied to solid-state nucleation in systems where mobility is limited. This timeline was expressed in terms of the ratio of the characteristic time for nucleation, $t_{\rm n}$, and the characteristic time for thermally-induced stochastic cluster formation (in the picture of CNT), $t_{\rm c}$. We suggested that the CNT approach to nucleation is more likely to be applicable at the right end of the timeline where $t_{\rm n}/t_{\rm c}\!>\!>\!1$, and that the geometric cluster model outlined in Section 2 is more likely to be a better representation at the left end of the timeline where $t_{\rm n}/t_{\rm c}\!<\!<\!1$. Indeed, we suggest that the two models represent two extremes on the $t_{\rm n}/t_{\rm c}$ spectrum and a transition between the two descriptions should be expected.

In all systems, both stochastic clusters (in the spirit of CNT) and geometric clusters can exist. Which type of cluster dominates the nucleation event will depend on their relative time scales for formation and lifetimes of existence. The geometric clusters emphasised in this contribution obviously have a formation time of zero - they are a statistical feature of the solution. At low temperatures, they are long-lived compared to the time for nucleation but they are not infinitely longlived. Individual clusters will exhibit a lifetime of $\tau=R^2/D$. Stochastic clusters, on the other hand, take time to form since they require mobility. Their formation is a strong function of the interfacial attachments rates and the long range diffusion rates, e.g. [3]. Depending on the relative time scales for the dissolution of geometric clusters and the formation of stochastic clusters, we should expect a transition from a description of nucleation dominated by geometric clusters (left end of time line in Fig. 3) to a description dominated by stochastic clusters (right end of timeline in Fig. 3). This transition will occur under different conditions in different systems and at different temperatures. In this respect, the geometric cluster model for nucleation should be seen as a complementary approach to CNT.

Since the geometric cluster model presented here does not consider stochastic cluster formation effects, it cannot, on its own, describe time-dependent nucleation (i.e. nucleation showing an incubation period due to the adjustment of the thermally-induced stochastic cluster size distribution). However, time-dependent nucleation is observed experimentally in some cases [3]. In such cases, either the incubation time has a physical origin other than the adjustment in the thermally-induced stochastic cluster size distribution, or the conditions of nucleation are

not at the left end of the timeline in Fig. 3, but closer to the centre or the right hand end of the timeline, where thermally-induced stochastic clusters are more important. Combining the types of analysis shown in Section 3 (competition in phase formation, and solvent trapping), where the geometric cluster model appears very successful, with detailed measurements of the nucleation rates and possible incubation times would provide valuable data to help identify transitions between the geometric cluster model and CNT, and to help position experimental conditions on the timeline shown in Fig. 3. It is likely conditions exist (e. g. in the middle of the timeline in Fig. 3) where features of both the geometric cluster model and CNT both play critical roles and this would be particularly interesting to probe experimentally.

5. Next steps

For problems of solid-state precipitation in engineering materials, a useful model for nucleation should be able to predict:

- which phase forms first, from the thermodynamically permissible phases
- the composition of the new phase that forms (i.e. any solvent trapping)
- the rate of formation (dN/dt) of the new phase
- the effect of structural & chemical heterogeneities
- how all the above depend on time, temperature and alloy composition

The geometric cluster model introduced in Section 2 has been shown to describe well the competition in phase nucleation (point #1), solvent trapping (point #2) and correctly describe the maximum number of precipitate particles (partially point #3), in several experimental systems (Al-Ni-Y, Cu-Co and Fe-Cu). In addition to greatly expanding the ranges of alloy systems for comparison, important next steps are integration of the above model into nucleation, growth and coarsening models for precipitation (e.g. KWM class models, e.g. [27–28]) so that quantitative nucleation rates can be compared with experimental data, especially regarding the temperature and bulk alloy content dependence.

In real alloy systems, defects also exist and we know these act as important heterogeneous nucleation sites. Introducing such effects into the geometric cluster model will be an important step for the future. One can easily imagine how strain and surface effects may modify the barrier for nucleation and the nuclei size, but the above model also provides a path for considering segregation effects (e.g. at dislocations). The basic idea of the geometric cluster model is that nucleation occurs in the matrix at locations where a nuclei-sized volume with the correct chemistry exists. This could include defects with segregation.

6. Conclusions

A new model for solid-state nucleation applicable to systems with limited mobility has been presented. This model emphasises the role of geometric clusters which are a statistical feature of the solution and not a result of thermally-induced stochastic fluctuations in the spirit of CNT. This model has been shown to successfully predict the competition in phase nucleation in a series of Al-Ni-Y glasses where the phase that forms first changes depending on the glass composition. It has also been shown to predict solvent trapping during the nucleation of solution phases and predicts maximum number densities of precipitates that agree well with experimental measurements.

CRediT authorship contribution statement

Christopher Hutchinson: Writing – review & editing, Writing – original draft, Visualization, Validation, Project administration, Methodology, Investigation, Funding acquisition, Formal analysis, Data

curation, Conceptualization. **Yves Brechet:** Writing – review & editing, Writing – original draft, Methodology, Formal analysis, Conceptualization.

Declaration of interests

The authors declare that they have no known competing financial interests or personal relationships that could have appeared to influence the work reported in this paper.

Acknowledgements

This work was supported by the Australian Research Council through the Discovery Projects Scheme (DP210102714). The authors are grateful for stimulating discussions with Prof Hatem Zurob (McMaster University).

References

- HI Aaronson, JK Lee, The kinetic equations of solid-solid nucleation theory and comparisons with experimental observations. Lectures On the Theory of Phase Transformations, TMS, Warrendale, PA, 1999.
- [2] E Clouet, Modelling of Nucleation Processes. ASM Handbook, Volume 22A: Fundamentals of Modeling for Metals Processing, DU Furrer and SL Semiatin, 2009, pp. 203–219. ASM International, Eds.
- [3] KF Kelton, AL Greer, Nucleation in Condensed Matter Applications in Materials and Biology, Pergamon, Oxford, 2010.
- [4] F de Geuser, MJ Styles, CR Hutchinson, A Deschamps, An in-situ combinatorial study of precipitation in composition gradients: experimental and modeling study in the Cu-Co system, Acta Mater. 101 (2015) 1–9.
- [5] Ed G Wilde, Early Stages of Crystal Formation in Glass-forming Metallic Alloys, in: W.P. Jü (Ed.), Glass: Selected Properties and Crystallization, De Gruyter, Inc, Schmelzer, 2014. Ed.
- [6] Y. Shen, JH Perepezko, Al-based amorphous alloys: Glass-forming ability, crystallization behaviour and effects of minor alloying additions, J. Alloy. Compd. 707 (2017) 3–11.
- [7] T Duan, Y Shen, SD Imhoff, F Yi, PM Voyles, JH Perepezko, Nucleation kinetics model for primary crystallization in Al-Y-Fe metallic glass, J. Chem. Phys. 158 (2023) 064504.
- [8] KF Kelton, GW Lee, AK Gangopadhyay, RW Hyers, TJ Rathz, JR Rogers, MB Robinson, DS Robinson, First x-ray scattering studies on electrostatically levitated metallic liquids: demonstrated influence of local icosahedral order on the nucleation barrier, Phys. Rev. Letts 90 (2003) 195504.
- [9] JE Spowart, DB Miracle, HM Mullens, The influence of solute distribution on the high nucleation density of Al crystals in amorphous aluminum alloys, J. Non-Crystall. Solid. 336 (2004) 202–211.

- [10] MJ Styles, MA Gibson, DR East, JA Kimpton, CR Hutchinson, On the competition in phase formation during crystallization of Al-Ni-Y metallic glasses, Acta Mater. 117 (2016) 170–187.
- [11] WJ Golumbfskie, PhD Thesis, The Pennsylvania State University, 2005.
- [12] WJ Golumbfskie, SN Prins, TJ Eden, ZK Liu, Predictions of the Al-rich region of the Al-Co-Ni-Y system based upon first-principles and experimental data, Calphad 33 (2009) 124–135.
- [13] JP Huang, B Yang, H Chen, H Wang, Thermodynamic optimization of the Ni-Y-Al ternary system, J. Phase Equilib. Diffus. 36 (2015) 357–365.
- [14] B Sonderegger, E Kozeschnik, Generalized nearest-neighbour broken-bond analysis of randomly oriented coherent interfaces in multicomponent fcc and bcc structures, Metall. Mater. Trans. A 40 (2009) 499–510.
- [15] A Deschamps, CR Hutchinson, Precipitation kinetics in metallic alloys: experiments & modelling, Acta Mater. 220 (2021) art117338.
- [16] WW Sun, RWK Marceau, MJ Styles, D Barbier, CR Hutchinson, G phase precipitation and strengthening in ultra-high strength ferritic steels: towards lean 'maraging' metallurgy, Acta Mater. 130 (2017) 28–46.
- [17] RP Setna, A Cerezo, JM Hyde, GDW Smith, Atomic-scale characterization of precipitation in copper-cobalt alloys, Appl. Surf. Sci. 76/77 (1994) 203–212.
- [18] A Cerezo, S Hirosawa, I Rozdilsky, GDW Smith, Combined atomic-scale modelling and experimental studies of nucleation in the solid-state, Phil. Trans. R Soc. Lond. A 361 (2003) 463–477.
- [19] A Morley, G Sha, S Hirosawa, A Cerezo, GDW Smith, Determining the compositions of small features in atom probe: bcc Cu-rich precipitates in an Fe-rich matrix, Ultramicroscopy 109 (2009) 535–540.
- [20] S Shu, BD Wirth, PB Wells, DD Morgan, GR Odette, Multi-technique characterization of the precipitates in thermally aged and neutron irradiated Fe-Cu and Fe-Cu-Mn model alloys: Atom probe tomography reconstruction implications, Acta Mater. 146 (2018) 237–252.
- [21] A Orthacker, G Haberfehlner, J Taendl, MC Poletti, B Sonderegger, G Kothleitner, Diffusion-defining atomic scale spinodal decomposition within nanoprecipitates, Nat. Mater. 17 (2018) 1101–1107.
- [22] E Clouet, Excess solvent in precipitates, Nat. Mater. 17 (2018) 1060-1061.
- [23] D Watanabe, C Watanabe, R Monzen, Determination of the interfacial energies of spherical, cuboidal and octahedral face-centred cubic precipitates in Cu-Co, Cu-Co-Fe and Cu-Fe alloys, Acta Mater. 57 (2009) 1899–1911.
- [24] H Guo, M Enomoto, CJ Shang, Simulation of bcc-Cu precipitation in ternary Fe-Cu-M alloys, Comp. Mat. Sci. 141 (2018) 101–113.
- [25] M Goune, P Maugis, E Pinto da Costa, D Bouleau, Precipitation of copper in ferrite: prediction of the strengthening kinetics, Rev. Met. Paris 101 (2004) 71–78.
- [26] CR Hutchinson, M Goune, A Redjaimia, Selecting non-isothermal heat treatment schedules for precipitation hardening systems: an example of coupled processproperty design, Acta Mater. 55 (2007) 213–223.
- [27] R. Kampmann, R. Wagner, Kinetics of precipitation in metastable binary alloys theory and application to Cu-1.9 at.% Ti and Ni-14 at. % Al. Decompos. Alloys Early Stages, Pergamon Press, Oxford, 1984.
- [28] M. Perez, M. Dumont, D. Acevedo-Reyes, Implementation of classical nucleation and growth theories for precipitation, Acta Mater. 56 (2008) 2119–2132.